

Supporting information for:

One-step synthesis of SBA-15 containing tungsten oxide nanoclusters: a chemoselective catalyst for oxidation of sulfides to sulfoxides at ambient conditions

Ankur Bordoloi^a, A. Vinu^b and S. B. Halligudi^{a,b*}

^a*Inorganic Chemistry & Catalysis Division,
National Chemical Laboratory,
Pune-411 008, India*

To whom correspondence to be addressed
Dr. S. B. Halligudi
Tel.: +91-20-25902107; Fax: +91-20-25902633
E-mail - sb.halligudi@ncl.res.in

^b*Nano-Ionics Materials Group, National Institute for Materials Science, 1-1,
Namiki, Tsukuba, Japan*

1. Experimental:

1.1. Chemicals

All the solvents procured from Merck (AR grade), India were distilled and dried prior to their use. All the sulfides and sulfoxides were purchased from Aldrich Chemicals and used as received.

1.2. Catalysts characterization

Tungsten content in the catalysts was determined by EDAX, using Microanalysis system (Model Phoenix, USA). Nitrogen adsorption and desorption isotherms were measured at -196 °C on a Quantachrome Autosorb 1 sorption analyzer. The samples were outgassed for 3 h at 250 °C under vacuum in the degas port of the adsorption analyzer. The specific surface area was calculated using the BET model. The pore size distributions were obtained from the adsorption branch of the nitrogen isotherms by Barrett-Joyner-Halenda method. The morphology and elemental mapping of the materials were observed on a Hitachi S-4800 field emission scanning electron microscope (HR-FESEM) with EDX using an accelerating voltage of 10 kV. The XRD patterns of the samples were collected on a Philips X'Pert Pro 3040/60 diffractometer using Cu K α radiation ($\lambda = 1.5418 \text{ \AA}$), iron as filter and X'celerator as detector. The HRTEM images and the

elemental mapping were observed on a JEOL Model 1200. The preparation of samples for HRTEM analysis involved sonication in ethanol for 5 min and deposition on a copper grid. The accelerating voltage of the electron beam was 120 kV. X-Ray photoelectron spectroscopy (XPS) measurements were performed on a VG Microtech Multilab ESCA 3000 spectrometer with a nonmonochromatized Mg-K α X-ray source. Energy resolution of the spectrometer was set at 0.8 eV with Mg-K α radiation at pass energy of 50 eV. The binding energy correction was performed using the C1s peak of carbon at 284.9 eV as a reference. Shimadzu FTIR-8201PC unit in DRS mode was used to obtain FTIR spectra of solid samples with a measurement range of 1400-700 cm⁻¹.

1.2.1. XPS and EDAX studies

The catalysts were characterized by X-ray photoelectron spectroscopy (XPS) and energy-dispersive X-ray analysis (EDAX) for the evaluation of their composition and purity. No peaks of any impurities such as metallic tungstate were detected in the XPS spectra of as-prepared WO_x nanoclusters, indicating the high purity of the material (Fig. 3S). The EDAX patterns of the materials (Fig. 2S) show the presence of W, Si and O peaks.

1.2.2. FTIR studies

FTIR spectroscopy in the skeletal region ranging between 1400-700 cm⁻¹ was employed to follow the variation behavior of the structure of WO_x/SBA-15. The typical bands due to siliceous material Si-O-Si are observed for both the parent and the WO_x/SBA-15 (Fig. 4S): a main band at 1080 cm⁻¹, with a shoulder at 1200 cm⁻¹ due to asymmetric Si-O-Si stretching modes and symmetric stretch at 805 cm⁻¹. Furthermore, an additional band at ca. 960 cm⁻¹ was observed. The band at 960 cm⁻¹ is widely used to characterize the presence of transition metal atoms near the silica framework as the stretching Si-O vibration mode perturbed by the neighboring metal ions. Thus the presence of such an infrared band due to perturbed silica vibrations can be attributed to the formation of WO_x nanoclusters in SBA-15.

1.2.3. SEM and TEM studies studies

SEM images show that the morphology of WO_x/SBA-15 remains the same as that of parent SBA-15 (Fig. 5S). HRTEM images display the presence of the hexagonally ordered pore system in WO_x/SBA-15. Moreover, a linear arrays of pores with a regular intervals is also observed, indicating that the structure of the SBA-15 is retained even after the formation of WO_x nanoclusters in the mesochannels.

1.2.3. Thermal stability of the catalyst system

A weight loss found in thermo gravimetric analysis (TGA) of calcined WO_x/SBA-15 sample below 373 K was due to the desorbed water (Fig. 6S).

1.3. Catalytic oxidation of sulfide

The liquid-phase catalytic oxidation of sulfides was conducted under atmospheric pressure at room temperature in 50 mol reaction vessel equipped with a magnetic stirrer. In a typical experiment, substrate (2 mmol) was oxidized using 70% TBHP (3 equiv) and catalyst (0.05 g) in CH₃OH: CH₂Cl₂ (1:1) (10 mL) at room temperature. The progress of the reaction was monitored by TLC and GC Shimadzu 14B gas chromatography (GC) with a capillary column (cross-linked 5% diphenyl–95% dimethylpolysiloxane capillary column, 30 m × 0.53 × 1.5 μm film thickness), coupled with flame ionization detector. After completion of the reaction, the reaction mixture was filtered off and the catalyst rinsed twice with CH₂Cl₂ (25-30 mL). The excess of solvent was removed under reduced pressure to give the corresponding pure sulfoxide (Table 1). In most cases, the products were analyzed without any chromatographic purification by GC (Shimadzu 14B) and GC-Mass spectroscopy (Shimadzu (GC-17A & QP-5000) with identical columns to obtain more than 99% conversions. All known reaction products gave satisfactory GC chromatogram and GCIR (Perkin Elmer system 2000) spectra as compared to those obtained from authentic samples. In case of di-*p*-tolylsulfoxides and *p*-nitrophenylmethylsulfoxides, after usual work-up, the crude sulfoxides were chromatographed on silica gel using solvent mixture hexane/ethyl acetate (10:1) as an eluent to afford the corresponding pure product confirmed by ¹H & ¹³C NMR (CDCl₃, 200 MHz).

1.3.1. Oxidation product of Methylphenylsulfide

The mixture was filtered to remove the catalyst and the solvent was removed under reduced pressure. It was then dried in *vacuo* and purified by column chromatography on silica as the stationary phase (petroleum ether/ethyl acetate, 50/50). Yield: 99%,

$^1\text{H NMR}$ (CDCl_3 , 200 MHz): $\delta = 7.47\text{--}7.53$ (m, 3H), 7.60–7.65 (m, 2H), 2.69 (s, 3H)

$^{13}\text{C NMR}$ (CDCl_3 , 200 MHz): $\delta = 131.1$ (C), 129.3 (CH), 128 (CH), 127.3 (CH), 125.3 (CH), 123.5 (CH), 44 (CH_3). **GCMS:** m/z 140(M^+), 125, 112, 97, 91, 77, 65, 51

1.4 Catalyst stability and Recyclability

To investigate the stability of $\text{WO}_x/\text{SBA-15}$ system towards a strong oxidant such as TBHP, two additional experiments were carried out. The spent catalyst $\text{WO}_x/\text{SBA-15}$ (after methylphenylsulfide oxidation process) was carefully separated from the reaction mixture and reused for methylphenylsulfide oxidation (second run). The decrease in the activity was insignificant. To check the effect of possible leaching of WO_x from the catalytic system, a fresh $\text{WO}_x/\text{SBA-15}$ sample was treated with a mixture of TBHP and $\text{CH}_3\text{OH}:\text{CH}_2\text{Cl}_2$ (1:1) under exactly the same conditions as the oxidation reaction (RT, 24 h). The liquid phase was carefully separated and analyzed for the presence of tungsten. The remaining solid was treated again with the mixture of $\text{CH}_3\text{OH}:\text{CH}_2\text{Cl}_2$ (1:1) and TBHP under the same conditions with subsequent analysis for tungsten. It was assumed that if partial leaching took place as a result of possible oxidation with TBHP, it should result in some release of tungsten. ICP-AES analysis of first and second treatment showed the absence of tungsten in the reaction mixture. These results indicate that 100 wt. % of WO_x still remains in the $\text{WO}_x/\text{SBA-15}$ system and there is no leaching of WO_x from this system even under drastic conditions. The $\text{WO}_x/\text{SBA-15}$ sample was also used after the first treatment with a fresh reaction mixture of $\text{CH}_3\text{OH}:\text{CH}_2\text{Cl}_2$ (1:1) and TBHP as catalyst for methylphenylsulfide oxidation. The decrease in catalytic activity was interestingly negligible up to tenth cycle. These results clearly show the practical reusability of the reported catalyst system under the described reaction conditions.

Table 1S: Physicochemical properties of catalyst systems

Entry	Materials	Surface area (m ² /g)	Pore Volume (cm ³ /g)	BJH _{Ads} (nm)
1	SBA-15	910	1.25	9.2
2	WO _x /SBA-15(2.5)	632	1.02	9.3
3	WO _x /SBA-15(5)	562	0.98	10.0
4	WO _x /SBA-15(10)	464	0.88	10.0
5	WO _x /SBA-15(20)	321	0.69	10.0

Table 2S: EDAX analysis data of catalyst systems

Entry	Materials	W		Si		O	
		wt%	At wt%	wt%	At wt%	wt%	At wt%
1.	SBA-15	0	0	38.1	26.0	61.9	74.0
2.	WO _x /SBA-15(2.5)	2.5	0.3	40.0	28.3	57.5	71.4
3.	WO _x /SBA-15(5)	8.1	0.9	34.7	25.5	57.2	73.6
4.	WO _x /SBA-15(10)	20.5	2.6	30.3	25.3	49.2	72.1
5.	WO _x /SBA-15(20)	36.9	5.8	26.6	27.6	36.5	66.6

Table 3S: Effect of the loading of WO_x on the activities of the SBA-15 catalysts in the oxidation of methylphenylsulfide

Entry	Catalysts	Yield (%)
1	SBA-15	0
2	$\text{WO}_x/\text{SBA-15}(2.5)$	7
3	$\text{WO}_x/\text{SBA-15}(5)$	19
4	$\text{WO}_x/\text{SBA-15}(10)$	28
5	$\text{WO}_x/\text{SBA-15}(20)$	55

Reaction conditions: Methylphenylsulfide (2 mmol) using 70% TBHP (3 equiv), catalyst weight 0.05 g in $\text{CH}_3\text{OH}:\text{CH}_2\text{Cl}_2$ (1:1) (10 mL), reaction temperature RT, and the reaction time 5h.

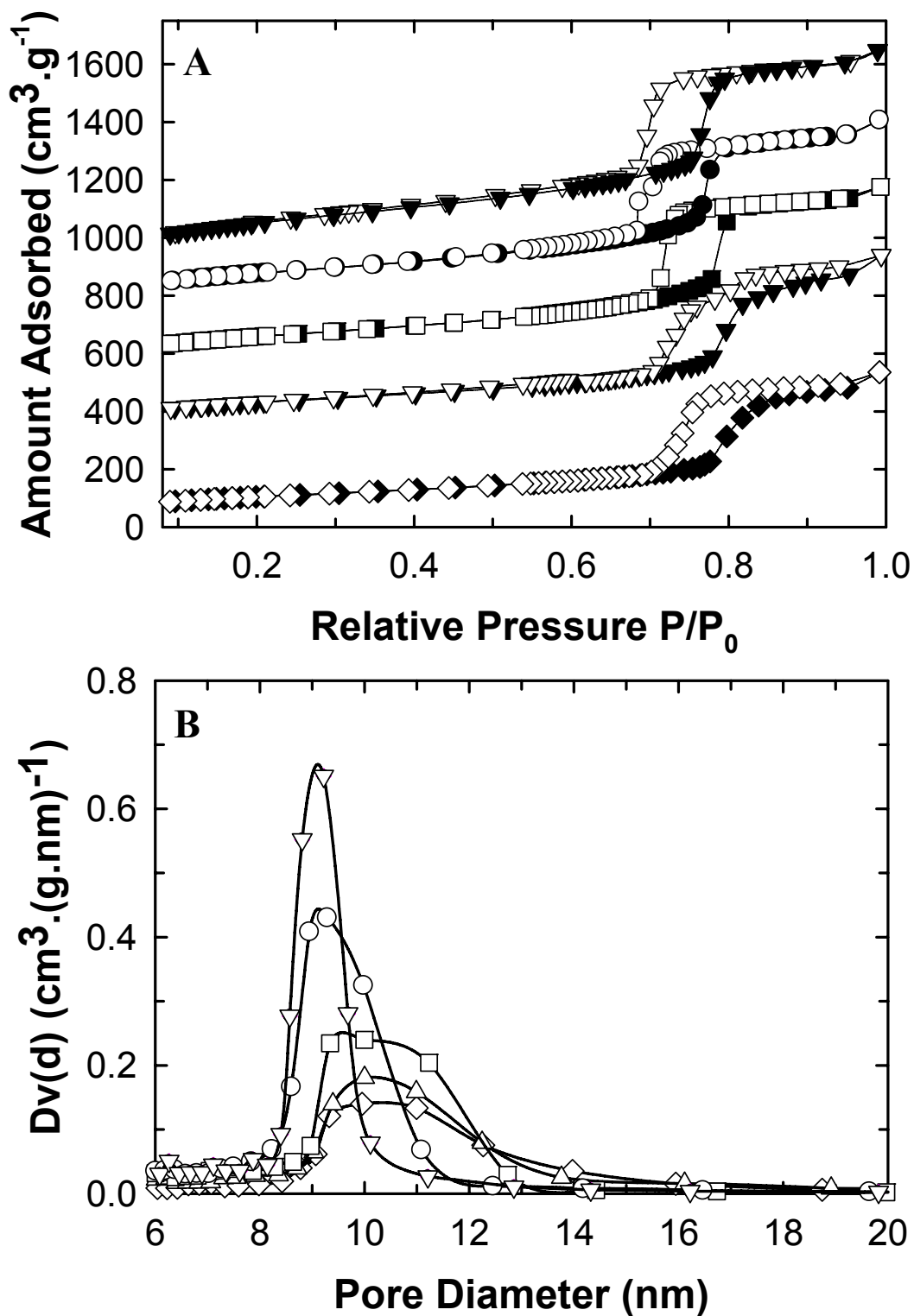


Figure 1S: (A) Nitrogen adsorption-desorption isotherms and (B) BJH adsorption pore size distributions of SBA-15 and WO_x/SBA-15: (Δ) SBA-15, (○) WO_x/SBA-15(2.5), (□) WO_x/SBA-15(5), (△) WO_x/SBA-15(10), and (◇) WO_x/SBA-15(20).

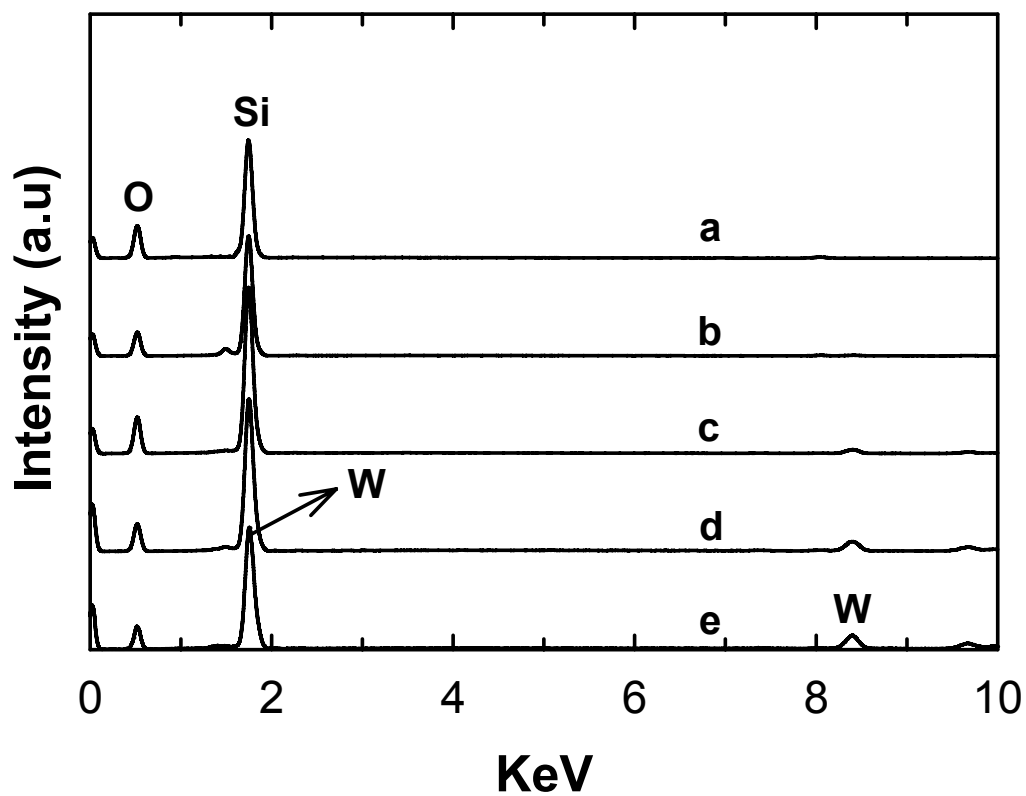


Figure 2S-1: HRSEM-EDS patterns of SBA-15 and $\text{WO}_x/\text{SBA-15}$: (a) SBA-15, (b) $\text{WO}_x/\text{SBA-15}(2.5)$, (c) $\text{WO}_x/\text{SBA-15}(5)$, (d) $\text{WO}_x/\text{SBA-15}(10)$, and (e) $\text{WO}_x/\text{SBA-15}(20)$.

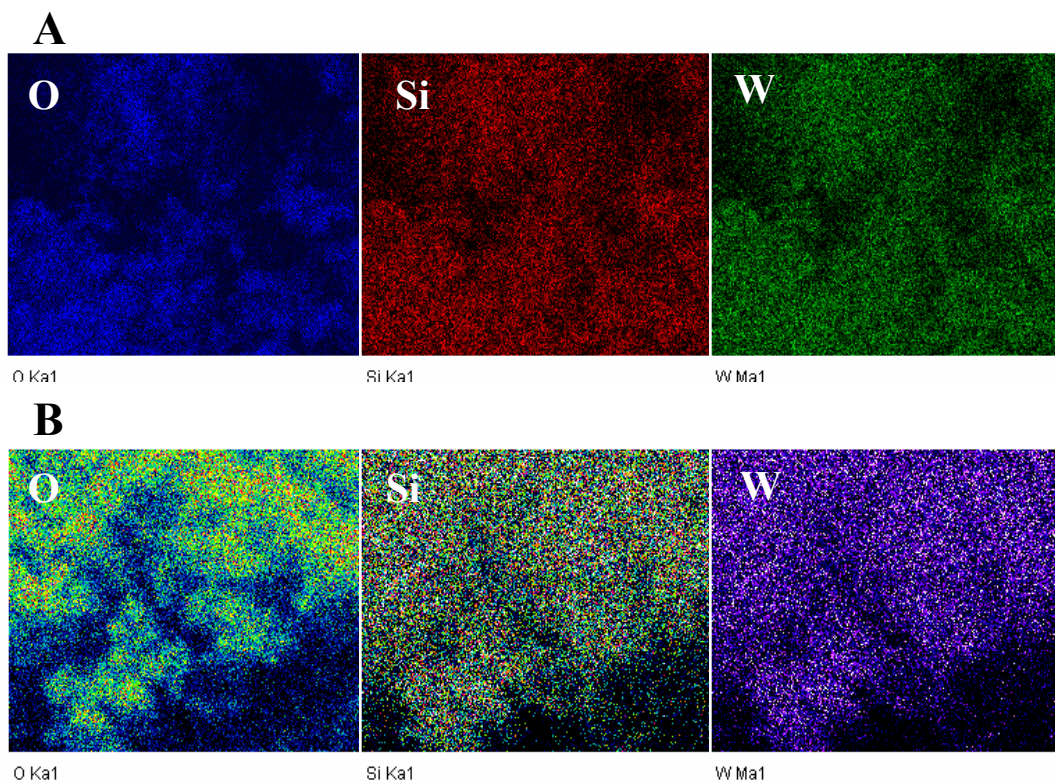


Figure 2S-2: Elemental mapping of (A) $\text{WO}_x/\text{SBA-15(20)}$, and (B) $\text{WO}_x/\text{SBA-15(5)}$.

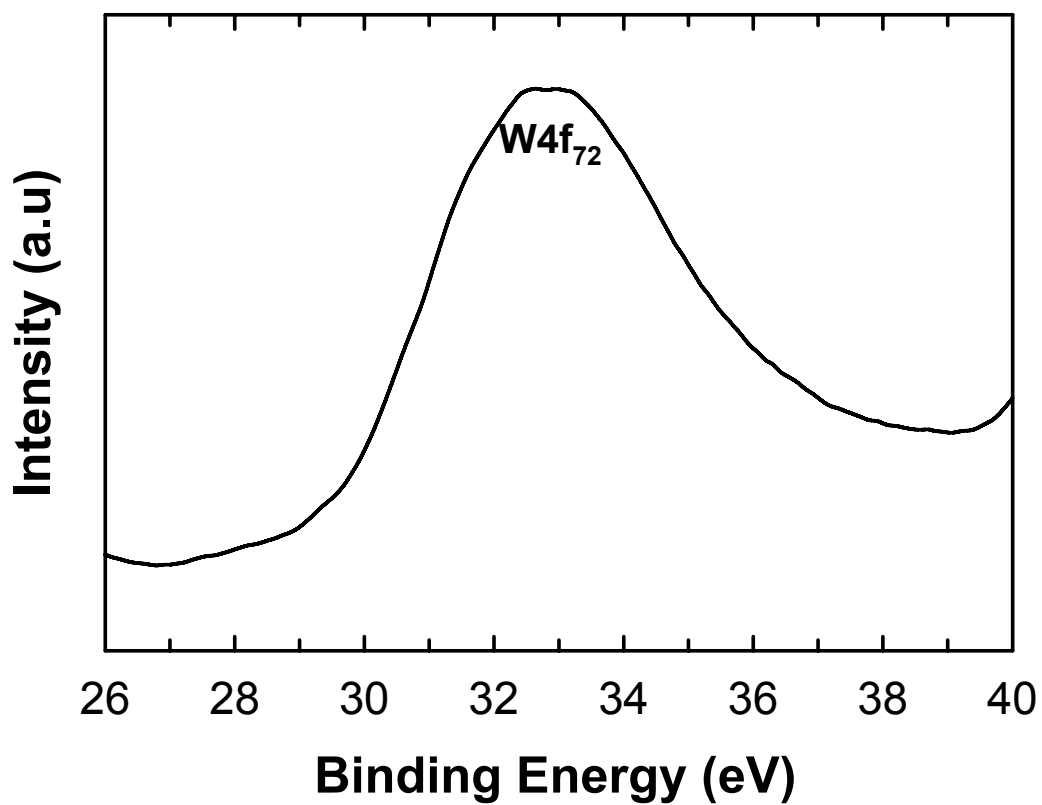


Figure 3S: XPS spectra of W(4f) of WO_x/SBA-15

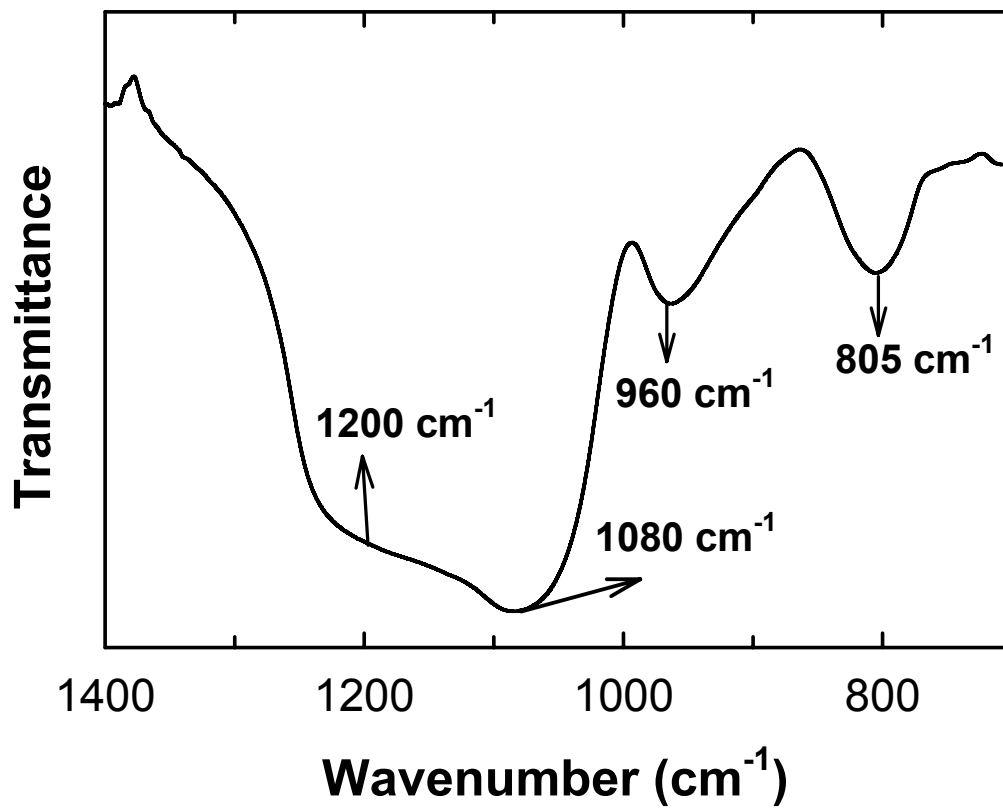


Figure 4S: FTIR spectrum of WO_x/SBA-15

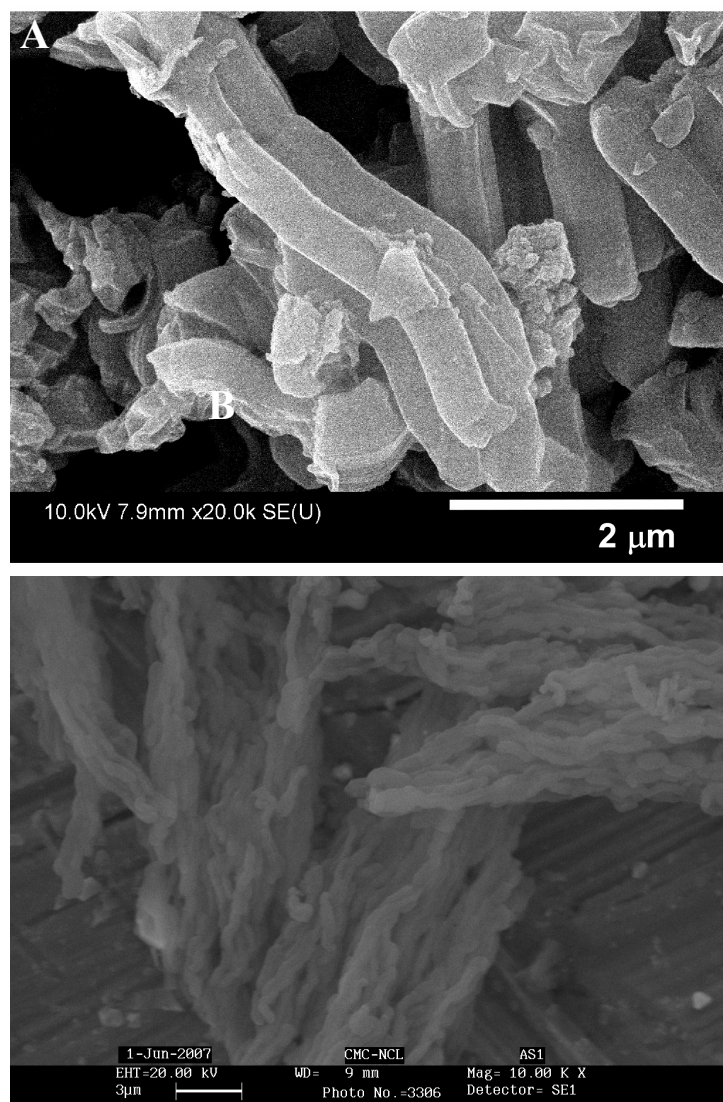


Figure 5S: HRSEM images of (a) SBA-15 and (b) WO_x/SBA-15

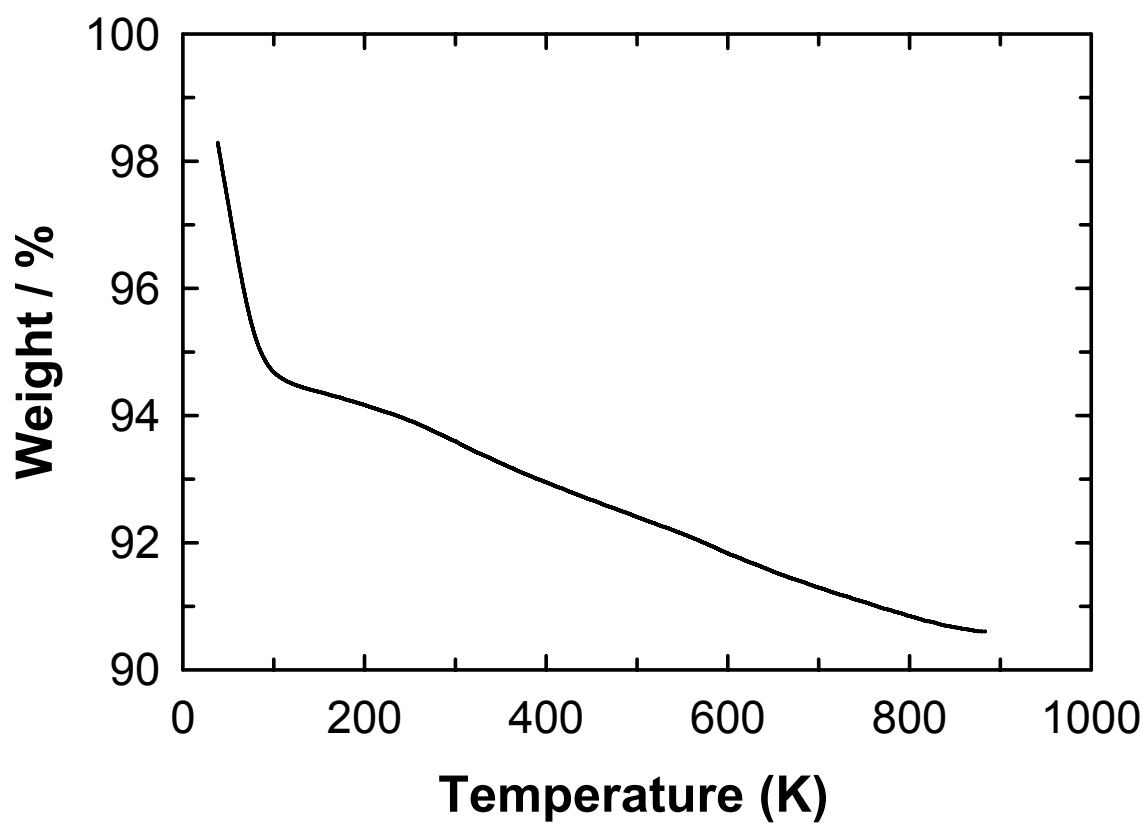


Figure 6S: TGA plot of WO_x/SBA-15